SAND98-1866J

Results of von Neumann Analyses for Reproducing Kernel Semi-discretizations

Mark A. Christon
Computational Physics R&D Department
and
Thomas E. Voth
Thermal Sciences Department

Sandia National Laboratories*
M/S 0819, P.O. Box 5800
Albuquerque, New Mexico 87185-0819
PH.: (505) 844-8520
FAX: (505) 844-0918
E-mail: machris@sandia.gov

submitted to:
International Journal for Numerical Methods in Engineering

July 31, 1998

*Sandia is a multiprogram laboratory operated by Sandia Corporation for the United States Department of Energy under Contract DE-AC04-94AL85000.

26p.

Abstract

The Reproducing Kernel Particle Method (RKPM) has many attractive properties that make it ideal for treating a broad class of physical problems. RKPM may be implemented in a "mesh-full" or a "mesh-free" manner and provides the ability to tune the method, via the selection of a window function and its associated dilation parameter, in order to achieve the requisite numerical performance. RKPM also provides a framework for performing hierarchical computations making it an ideal candidate for simulating multi-scale problems. Although the method has many appealing attributes, it is quite new and its numerical performance is still being quantified with respect to more traditional discretization techniques. In order to assess the numerical performance of RKPM, detailed studies of the method on a series of model partial differential equations has been undertaken. The results of von Neumann analyses for RKPM semi-discretizations of one and two-dimensional, first and second-order wave equations are presented in the form of phase and group errors. Excellent dispersion characteristics are found for the consistent mass matrix with the proper choice of dilation parameter. In contrast, row-sum lumping the mass matrix is demonstrated to introduce severe lagging phase errors. A "higher-order" mass matrix improves the dispersion characteristics relative to the lumped mass matrix but also yields significant lagging phase errors relative to the fully integrated, consistent mass matrix.

Key Words: reproducing kernel particle methods, meshless, dispersion

1 Introduction

The accurate simulation of wave propagation or advection dominated processes using discrete numerical schemes hinges upon having a clear understanding of the constraining numerical errors, and sufficient computational resources to effect solutions at the requisite grid scale. Examples of this may be seen when attempting to simulate wave propagation in an acoustic medium, or compute turbulent flow fields via direct numerical simulation (DNS) or large eddy simulation (LES). In physical problems with a dominant hyperbolic character, controlling the dispersive errors, i.e., phase and group speed errors, to within 5% can require 8 to 10 grid points per wavelength with traditional finite difference or lumped-mass finite element methods. Thus,

the simulation of hyperbolic problems is limited by the wavelength that the grid can accurately represent. Further, a failure to respect the so-called grid Nyquist limit can introduce deleterious aliasing effects that corrupt the simulation fidelity.

An alternative to traditional grid-based approaches is the class of methods based on moving least-squares, reproducing kernels, and partitions of unity. An overview of the development of these methods is presented by Belytschko, et al.[1] The methods based upon reproducing kernels are of interest here because they promise to deliver enhanced numerical performance on a broad range of physical problems and provide a framework for incorporating multiresolution analysis.

Liu and his co-workers have been developing reproducing kernel particle methods for a number of years and have demonstrated applications ranging from structural acoustics to large deformation mechanics problems.[10–12,15] In addition, Liu, et al.[9,17] have combined reproducing kernel ideas with multiresolution analysis using wavelets, permitting the decomposition of discrete solutions into multiple scales. The application of RKPM to structural dynamics has been demonstrated by Liu, et al.[14] in addition to showing that the reproducing kernel interpolation functions satisfy necessary consistency conditions. Uras, et al.[18] have applied RKPM to acoustics problems demonstrating that the dilation parameter in the window function may be used to perform the RKPM analogue of "h-p adaptivity".

In a series of papers by Liu and Li[6,8,16] moving least squares reproducing kernel methods are developed beginning with the basic formulation and continuing through a Fourier analysis and the incorporation of wavelet packets. The possibility for RKPM to deliver synchronized rates of convergence for the discrete functions and their derivatives has also been explored by Li and Liu.[7] The application of RKPM to nearly incompressible, hyper-elastic solids was considered by Chen, et al.,[2] while the treatment of large deformation problems has been explored by Liu, et al.[5,13] The enrichment of finite element computations with RKPM has also been addressed permitting local regions of the computational domain to be treated with RKPM while the global problem is treated with a standard finite element formulation.[3]

Although the application of RKPM has been demonstrated on a broad class of problems, its numerical performance has not been quantified with respect to more traditional methods. Here, numerical performance is broadly defined to include truncation error, consistency and stability, rate of convergence, dispersive character, and spatial adaptivity. In order to apply numer-

ical methods such as RKPM to wave propagation or advection dominated problems and faithfully represent the physics, a clear understanding of the phase and group errors associated with the numerical method is necessary.

In general, the application of discrete methods to hyperbolic partial differential equations can result in solutions that are dispersive even though the physical model for wave propagation is non-dispersive. Dispersion errors are typically characterized by the differences between the apparent, i.e., numerical, phase and group speed of waves and their exact counterparts. Phase and group speed errors represent some of the most constraining numerical errors associated with the simulation of wave propagation and advection dominated flows.

In the context of linear acoustics, the phase speed is the speed at which individual waves propagate. In the absence of dispersion, i.e., for a perfect acoustic fluid, this is simply the sound speed. In a dispersive acoustic medium, the phase speed is a function of the frequency or wavelength of the propagating wave. Thus, phase error may be viewed as a measure of the influence of numerical dispersion on the apparent sound speed relative to the true sound speed.

In contrast to the phase speed, the group speed describes the propagation of wave packets that are comprised of short wavelength signals modulating a slowly varying, longer wavelength envelope. Because the energy associated with a wave packet travels with the packet, the group speed is often referred to as the "energy" velocity. The group speed is also referred to as the speed of modulation. For a non-dispersive medium the phase and group speed are identical.

In discrete wave propagation problems, the group speed may be used to study and explain the propagation of short wavelength oscillations that are typically $2\Delta x$ in wavelength where Δx is the characteristic mesh spacing. Vichnevetsky[19,20] has demonstrated that spurious $2\Delta x$ oscillations, that are induced by rapid changes in mesh resolution and at physical boundaries, propagate at a group speed associated with a $2\Delta x$ wavelength.

The investigation of the dispersive errors associated with discrete solutions is not new and has been used by numerous researchers to characterize the performance of numerical methods. A brief review of earlier dispersion analyses may be found in Christon.[4] The focus of the current work is upon characterizing the dispersive nature of the reproducing kernel particle method for hyperbolic problems.

In the following sections, an overview of the dispersion analysis and a sum-

mary of the formulae for computing the phase and group speed for RKPM semi-discretizations of the first and second-order wave equations are presented. In section 3, the phase and group speed for both consistent, lumped, and higher-order mass matrices are presented for both finite element and RKPM semi-discretizations. Finally, the results of the dispersion analysis are summarized and conclusions are drawn.

2 Formulation

This section begins with a brief overview of the reproducing kernel particle method. A detailed presentation of RKPM is beyond the scope of this paper, and the reader is directed to the literature for details concerning the method.[2,3,5–18] Following the overview is a derivation of the formulae for computing the normalized phase and group speed associated with semi-discretizations of the model hyperbolic partial differential equations.

2.1 Reproducing Kernel Particle Formulation

For the sake of clarity, the following overview is limited to one spatial dimension although the formulation may be easily extended to higher dimensions.[2,11,12] The RKPM formulation begins with the notion of a kernel approximation of a function, U, on a domain, Ω,

$$U^R(x) = \int_\Omega U(\xi)\varphi(x-\xi)d\xi, \tag{1}$$

where φ is the kernel function and U^R is the continuous approximation to U.[11,15] In order to address discrete problems, numerical quadrature (i.e., trapezoidal or particle integration) is used to evaluate Eq. (1) as

$$U^h(x) = \sum_{i=1}^{Np} d_i\varphi(x-x_i)\Delta x_i, \tag{2}$$

where U^h is the discrete analogue of U^R, d_i are the particle coefficients, and Np is the total number of particles in the domain, Ω.[11] In general, the coefficients, d_i, are different from the value of the function at particle i because the RKPM basis is non-nodal, i.e., it does not posses the Kronecker-delta property.

One of the most commonly used RKPM kernel functions, and the one used here, is the cubic spline. In one-dimension, the cubic spline kernel function is

$$\varphi(z) = \begin{cases} \frac{2}{3r\Delta x}\left[1 - \frac{3}{2}z^2 + \frac{3}{4}z^3\right] & z < 1 \\ \frac{1}{6r\Delta x}\left[2 - z\right]^3 & 1 \leq z < 2, \\ 0 & z \geq 2 \end{cases} \tag{3}$$

where $z = |x - x_i| / (r\Delta x)$, x_i is the position of particle i, Δx is the particle spacing, and r is the refinement parameter.[1,11,12] The refinement parameter controls the dilation of the kernel function, and subsequently, the domain of influence for the function. For example, consider the cubic-spline window function with a uniform particle distribution. In this case, $r = 1/2$ results in support over 3 particles, while $r = 1$ results in support over 5 particles. In this work, the optimal dilation parameter, $r = 1.14$, established by Liu and Chen[9] to minimize aliasing error in terms of energy, is used.

In general, Eq. (2) will not exactly reproduce an arbitrary polynomial. The accurate reproduction of polynomials to order p is ensured by introducing a modified window function,

$$\overline{\varphi}(x - x_i) = \sum_{k=0}^{p} \beta_k(x)\varphi(x - x_i)\,(x - x_i)^k, \tag{4}$$

where $\beta_k(x)$ represents a set of correction functions that vary within the domain, Ω.[11,12] The modified window function, $\overline{\varphi}$, replaces φ in Eq. (2) yielding

$$U^h(x) = \sum_{i=1}^{Np} \overline{\varphi}(x - x_i) d_i \Delta x_i. \tag{5}$$

The correction functions are determined by substituting Eq. (4) into Eq. (5) and requiring that the resulting kernel approximation reproduce polynomials to the desired order. For linear consistency, the following constraints are required.

$$\sum_{i=1}^{Np} \left[\beta_0(x) + \beta_1(x)\,(x - x_i)\right] \varphi(x - x_i)\Delta x_i = 1 \tag{6}$$

$$\sum_{i=1}^{Np} \left[\beta_0(x) + \beta_1(x)\,(x - x_i)\right] \varphi(x - x_i) x_i \Delta x_i = x \tag{7}$$

From these equations, $\beta_0(x)$ and $\beta_1(x)$ may be calculated in a point-wise fashion in the domain. With the correction functions in hand, the requisite derivatives for a Bubnov-Galerkin procedure may be computed. Although the calculation of these derivatives is rather straight forward, the algebra required is significant and the reader is directed to the work of Liu, et al.[2,11,12] for details.

Remark

> As a brief aside, consider the limiting case where the linear "hat function" is used as the kernel function instead of the cubic-spline of Eq. (3). In this case, the window function is
>
> $$\varphi(z) = \begin{cases} \frac{1-z}{r\Delta x} & z < 1 \\ 0 & z \geq 1 \end{cases} \tag{8}$$
>
> If the dilation parameter is unity, then the resulting basis elements are simply the linear finite element functions and yield the usual form of the mass and stiffness operators.

In the ensuing dispersion analysis, tensor products of Eq. (3),

$$\tilde{\varphi}\left(\frac{x-x_i}{r\Delta x}, \frac{y-y_j}{r\Delta y}\right) = \varphi\left(\frac{x-x_i}{r\Delta x}\right)\varphi\left(\frac{y-y_j}{r\Delta y}\right), \tag{9}$$

are used to generate a two-dimensional kernel function with rectangular support.[1,12] The tensor-product kernel function in Eq. (9) is used with bi-linear consistency enforced for the two-dimensional dispersion results presented in section 3.

2.2 von Neumann Analysis

With the RKPM formulation outlined, the weak forms of two model partial differential equations are presented with a brief description of the Fourier analysis. To begin, the two-dimensional first and second-order wave equations are, in Cartesian coordinates,

$$\frac{\partial U}{\partial t} + c_x\frac{\partial U}{\partial x} + c_y\frac{\partial U}{\partial y} = 0 \tag{10}$$

and,

$$\frac{\partial^2 U}{\partial t^2} - c^2 \left[\frac{\partial^2 U}{\partial x^2} + \frac{\partial^2 U}{\partial y^2} \right] = 0, \tag{11}$$

where t is time, U is the unknown variable, c is the wave speed and $(c_x, c_y) = (c\cos(\theta), c\sin(\theta))$ are the advection velocity components, and θ is the advection direction measured from the x-axis. The semi-discrete forms of Eq. (10) and (11) are required for the following analysis. The details for obtaining the weak form of these equations are well known, and are not repeated here. The semi-discrete forms of the first and second-order wave equations are

$$\mathbf{M}\dot{\mathbf{d}} + \mathbf{A}\mathbf{d} = \mathbf{0}, \tag{12}$$

and

$$\mathbf{M}\ddot{\mathbf{d}} + \mathbf{K}\mathbf{d} = \mathbf{0}, \tag{13}$$

where $\mathbf{A}$ is the advection operator, $\mathbf{K}$ is the stiffness matrix and $\mathbf{d}$ is a vector of unknown coefficients. In this analysis, a generalized mass matrix is used,

$$\mathbf{M} = \alpha \mathbf{M}^c + (1-\alpha)\mathbf{M}^l, \tag{14}$$

where $\mathbf{M}^c$ and $\mathbf{M}^l$ are the consistent and row-sum-lumped mass matrices respectively, and $0 \leq \alpha \leq 1$.

Proceeding with the Fourier analysis, a plane wave solution is placed on an infinite span (alternatively, on a finite domain with periodic boundary conditions) in order to compare the exact and semi-discrete solutions. It can be shown that the particle values, $\mathbf{U}^h$, satisfy the same evolution equations as the coefficients, $\mathbf{d}$, when a periodic domain and symmetric window functions are used.[20] Thus, Eq. (12) and (13) may be rewritten in terms of $\mathbf{U}^h$ for the purposes of this analysis, and the plane wave solution to Eq. (10) and (11) may be expressed as

$$U(x, y, t) = U_0 \exp[\iota k(x\cos(\theta) + y\sin(\theta)) - \iota\omega t]. \tag{15}$$

Here, U_0 is the amplitude, k is the wave number, θ is the propagation direction of a plane wave measured from the x-axis, and $\iota = \sqrt{-1}$.

Now, considering the regular distribution of particles shown in Figure 1, any particle $(i+m, j+n)$ at coordinates (x_{i+m}, y_{j+n}) may be located relative any other particle (i, j) in terms of the particle spacing Δx, Δy. With the

particle spacing defined, the generalized solution to the semi-discrete model equations is

$$U_{i+m,j+n} = U_{i,j} \exp[\iota k(m\Delta x \cos\theta + n\Delta y \sin\theta)], \tag{16}$$

where $U_{i,j} = U_0 \exp[\iota k(x_i \cos\theta + y_j \sin\theta) - \iota\omega t]$.

For a kernel function with arbitrary support, the semi-discrete forms of the first and second-order wave equations may be rewritten for particle (i, j) as

$$\sum_{l=-n}^{n} \sum_{m=-n}^{n} \left\{ M_{(i,j),(i+l,j+m)} \dot{U}_{i+l,j+m} + A_{(i,j),(i+l,j+m)} U_{i+l,j+m} \right\} = 0, \tag{17}$$

and

$$\sum_{l=-n}^{n} \sum_{m=-n}^{n} [M_{(i,j),(i+l,j+m)} \ddot{U}_{i+l,j+m} + K_{(i,j),(i+l,j+m)} U_{i+l,j+m}] = 0, \tag{18}$$

where $M_{(i,j),(i+l,j+m)}$, $K_{(i,j),(i+l,j+m)}$ and $A_{(i,j),(i+l,j+m)}$ are the mass, stiffness and advection matrix entries on the row associated with particle (i, j) and the column associated with particle $(i + l, j + m)$. Here, the summation is over the range of all particles under the support of the kernel function at particle (i, j).

Substituting Eq. (16) and its associated temporal derivatives into Eq. (17) and (18), equations for the circular frequency, ω, in terms of the wavenumber, wave propagation direction and particle spacing are obtained for the first and second-order equations respectively.

$$\begin{aligned} -i\omega \sum_{l=-n}^{n} \sum_{m=-n}^{n} & [M_{(i,j),(i+l,j+m)} \exp(\iota k(l\Delta x \cos(\theta) + m\Delta y \sin(\theta)))] + \\ & \sum_{l=-n}^{n} \sum_{m=-n}^{n} A_{(i,j),(i+l,j+m)} \exp(\iota k(l\Delta x \cos(\theta) + m\Delta y \sin(\theta))) = 0 \end{aligned} \tag{19}$$

$$\begin{aligned} -\omega^2 \sum_{l=-n}^{n} \sum_{m=-n}^{n} & [M_{(i,j),(i+l,j+m)} \exp(\iota k(l\Delta x \cos(\theta) + m\Delta y \sin(\theta)))] + \\ & \sum_{l=-n}^{n} \sum_{m=-n}^{n} [K_{(i,j),(i+l,j+m)} \exp(\iota k(l\Delta x \cos(\theta) + m\Delta y \sin(\theta)))] = 0 \end{aligned} \tag{20}$$

The computation of the normalized phase and group speed proceeds by solving for the circular frequency, ω, and making use of the fact that for a non-dispersive medium, $c = \omega/k$. The normalized phase speed is defined as $\psi = \bar{c}/c$ where $\bar{c}$ is the discrete phase speed. Rearranging Eq. (19) and (20) yields

$$\psi_1 = \frac{1}{\iota ck} \frac{\sum_{l=-n}^{n} \sum_{m=-n}^{n} [A_{(i,j),(i+l,j+m)} \exp(\iota k(l\Delta x \cos(\theta) + m\Delta y \sin(\theta)))]}{\sum_{l=-n}^{n} \sum_{m=-n}^{n} [M_{(i,j),(i+l,j+m)} \exp(\iota k(l\Delta x \cos(\theta) + m\Delta y \sin(\theta)))]} \tag{21}$$

and

$$\psi_2 = \frac{1}{ck} \sqrt{\frac{\sum_{l=-n}^{n} \sum_{m=-n}^{n} [K_{(i,j),(i+l,j+m)} \exp(\iota k(l\Delta x \cos(\theta) + m\Delta y \sin(\theta)))]}{\sum_{l=-n}^{n} \sum_{m=-n}^{n} [M_{(i,j),(i+l,j+m)} \exp(\iota k(l\Delta x \cos(\theta) + m\Delta y \sin(\theta)))]}} \tag{22}$$

for the first and second-order wave equations respectively.

The one-dimensional phase speed can be obtained from the two-dimensional formulae by simply setting $\theta = 0$. Assuming that the kernel function is symmetric so that $\mathbf{M}^c$ and $\mathbf{K}$ are symmetric and $\mathbf{A}$ is anti-symmetric, the phase speed for the first and second-order, one-dimensional semi-discretizations are

$$\psi_1 = \frac{f_a}{ck f_m}, \tag{23}$$

and

$$\psi_2 = \frac{1}{ck} \sqrt{\frac{f_k}{f_m}}, \tag{24}$$

where

$$f_a = A_{i,i} + 2 \sum_{l=1}^{n} \sin(kl\Delta x) A_{i,i+l}, \tag{25}$$

$$f_m = M_{i,i} + 2 \sum_{l=1}^{n} \cos(kl\Delta x) M_{i,i+l}, \tag{26}$$

and

$$f_k = K_{i,i} + 2 \sum_{l=1}^{n} \cos(kl\Delta x) K_{i,i+l}. \tag{27}$$

The normalized group speed, in one-dimension, is defined as $\zeta = v_g/c$, where $v_g = \partial\omega/\partial k$. Consideration of the normalized group velocity for the

two-dimensional semi-discretizations introduces significant complexities that make such analysis beyond the scope of this work.

Using Eq. (23) and (24), the normalized group speed in one-dimension is

$$\zeta_1 = \frac{g_a f_m - f_a g_m}{c f_m^2}, \tag{28}$$

and

$$\zeta_2 = \frac{\sqrt{f_m}}{2c\sqrt{f_k}} \frac{g_k f_m - f_k g_m}{f_m^2} \tag{29}$$

for the first and second-order wave equations respectively. Here,

$$g_a = \partial f_a / \partial k = 2\Delta x \sum_{l=1}^{n} l \cos(kl\Delta x) A_{i,i+l} \tag{30}$$

$$g_m = \partial f_m / \partial k = -2\Delta x \sum_{l=1}^{n} l \sin(kl\Delta x) M_{i,i+l}, \tag{31}$$

and

$$g_k = \partial f_k / \partial k = -2\Delta x \sum_{l=1}^{n} l \sin(kl\Delta x) K_{i,i+l}. \tag{32}$$

Remark

> There have been no restrictions (other than symmetry) placed on the form or type of basis functions used to obtain the mass, stiffness or advection operators. Thus, Eq. (21) through (29) are equally valid for Galerkin formulations that use the RKPM functions or finite element basis functions.

3 Results

This section summarizes the results of the von Neumann analyses in terms of phase and group speed for RKPM semi-discretizations of the one-dimensional model hyperbolic equations followed by phase speed associated with the two-dimensional equations. Unless otherwise noted, the normalized phase and group speeds defined in the previous section are referred to simply

as phase and group speed in the remaining text. Both the one and two-dimensional RKPM formulations use the cubic spline kernel function in Eq.(3). Further, the two dimensional formulation uses the tensor product in Eq. (9) to produce a two dimensional kernel function. Both spatial formulations use the procedure outlined in Section 2.1 to generate modified window functions that ensure linear ($U(x) = 1 + x$; one-dimensional) and bi-linear ($U(x, y) = 1 + x + y + xy$; two-dimensional) functions are reproduced exactly.

For the purpose of comparison, results are presented for linear and bi-linear finite element (FE) semi-discretizations. Here, the linear and bi-linear finite element basis functions where chosen for comparison as they provide the same order of consistency as the RKPM discretizations considered. The FE phase and group speed are calculated using the formulae presented in Section 2.2 with linear finite element basis functions.

In the discussion that follows, the phase and group speed results are presented as functions of non-dimensional wave number, $k\Delta x/\pi = 2\Delta x/\lambda$. In order to simplify the discussion, the following nomenclature has been adopted to identify the the mass matrix and quadrature rule used for both the FE and RKPM results. The mass matrix is identified as C for consistent ($\alpha = 1$), L lumped ($\alpha = 0$), or H higher-order ($\alpha = 1/2$); cf. Eq. (14). The numerical integration scheme is identified as either F indicating full Gauss quadrature, or T indicating a trapezoidal rule, i.e., particle integration.

The F nomenclature for "full Gauss quadrature" indicates a 2×2 quadrature rule for the bi-linear finite element and a 4×4 quadrature rule for the RKPM formulation. In the case of the RKPM formulation, the sensitivity of the matrix entries with respect to the quadrature rule was tested and demonstrated that the entries did not change with increased number of quadrature points beyond 4×4. For trapezoidal (particle) integration, the particle locations are used as quadrature points. Here, the motivation for consideration of particle integration is the potential reduction in computational complexity gained by elimination of the background integration mesh which also results in a truly mesh-free method.

3.1 One-Dimensional Hyperbolic Equations

In this section, the phase and group speed for the semi-discrete, one-dimensional, first and second-order wave equations are presented.

3.1.1 First-Order Wave Equation

Phase and group speed for the linear finite element semi-discretizations of the first-order wave equation are presented in Figure 2. Results are plotted for fully integrated, consistent (CF), lumped (LF) and higher-order (HF) mass matrix formulations. As shown, the FE formulations introduce strictly lagging phase speed for all wavelengths considered with the CF formulation delivering smaller phase errors up to the $2\Delta x$ limit. All three mass matrices result in a phase speed of zero at $2\Delta x/\lambda = 1$, i.e., wavelengths of $2\Delta x$ are stationary on the grid.

The finite element discretizations also yield strictly lagging group speed for all three mass matrices. However, the lumped mass matrix yields a zero group speed for $4\Delta x$ wavelengths while both the CF and HF mass matrices have zero group speed at shorter wavelengths. The CF formulation performs better than the LF and HF formulations, i.e., yields smaller group errors for $\lambda \geq 3\Delta x$. All three formulations yield negative group speeds for short wavelengths indicating that the energy associated with $2\Delta x$ wavelength signals propagates in the opposite direction of the longer wavelength signals. Surprisingly, the LF formulation yields the smallest, albeit still negative group speed in the limit of $2\Delta x$ wavelengths.

Figure 3 shows the phase and group speed for the one-dimensional RKPM semi-discretizations of the first-order wave equation. Again, fully integrated consistent (CF), lumped (LF) and higher-order (HF) mass matrix formulations are presented. In addition, results are shown for the consistent mass matrix formulation with particle integration of the advection and mass matrices (CT). As with the FE results in Figure 2, the RKPM method introduces lagging phase errors over the discrete spectrum of wavelengths. The consistent mass (CF) formulation performs the best and delivers significantly better phase speed relative to the FE results presented in Figure 2. In order to quantify the increased performance of the RKPM-CF method, consider a phase error, $\epsilon = |1 - \psi|$, of 5% or less to be appropriate for engineering purposes. For the FE-CF method, this criterion corresponds to $4\Delta x$ or 5 grid-points per wavelength. In contrast, the RKPM-CF and CT methods require $2 - 3\Delta x$, or approximately $3 - 4$ particles per wavelength. While both the RKPM-CF and CT methods perform quite well, the lumped and higher-order formulations introduce severe lagging phase errors relative to their finite element counterparts.

In terms of the group speed, both the RKPM-CT and CF formulations

are far superior to the LF and HF formulations. Similar to the phase speed, the CT formulation yields lagging group errors at longer wavelengths than the CF formulation. However, the trapezoidal mass matrix, CT, avoids the large negative group speed associated with the fully-integrated, CF, matrix at $2\Delta x$ wavelengths. Both the FE-CF and RKPM-CT formulations yield negative group speed for wavelengths shorter than $3\Delta x$, while the RKPM-CF formulation produces negative group speed for wavelengths shorter than about $2.5\Delta x$. However, the group error associated with $2\Delta x$ wavelengths for the RKPM-CF formulation is over 3 times larger than for the FE-CF case and is 10 times larger than the sound speed. From these results it is apparent that the RKPM-CT and CF formulations exhibit very good dispersive behavior, discounting the large negative group speed for the RKPM-CF case, with consistency identical to the finite element formulation.

3.1.2 Second-Order Wave Equation

Phase and group speeds for the linear finite element semi-discretizations of the second-order wave equation are presented in Figure 4 for the fully integrated, consistent, lumped and higher-order mass matrix formulations. The consistent mass formulation (CF) introduces leading phase errors while the lumped (LF) and higher-order (HF) methods exhibit strictly lagging phase errors. Additionally, both the LF and HF methods demonstrate lagging group speed for all wavelengths considered while the CF group speed is leading for $2\Delta x/\lambda \leq 0.85$.

Figure 5 shows the phase and group speeds for the one-dimensional, second-order wave RKPM semi-discretization using the CF, CT, LF and HF formulations. Relative to the FE results of Figure 4, the consistent mass matrix (CF) provides better phase and group speed. Surprisingly, the trapezoidal mass formulation (CT) yields zero phase speed for $2\Delta x$ wavelengths, i.e., these wavelengths are stationary on the grid. Additionally, the CT formulation results in large, lagging group errors for wavelengths shorter than $3\Delta x$. In contrast, the FE semi-discretizations do not yield any negative group speeds.

Employing the 5% phase error criterion introduced earlier, the FE-HF method requires approximately 4 nodes per wavelength while only 3 particles are required for the RKPM-CF method. As with the RKPM discretization of the first-order wave equation, the lumped and higher-order formulations introduce severe lagging phase and group errors relative to both the FE

counterparts and the CT and CF mass matrices.

3.2 Two-Dimensional Hyperbolic Equations

This section presents the phase speed results for the semi-discrete, two-dimensional, hyperbolic equations. Results are plotted as functions of the propagation angle, θ, and non-dimensional wave number. For this analysis, the particle spacing is uniform with, $\Delta y/\Delta x = 1$. As with the one-dimensional analyses, a refinement parameter of $r = 1.14$ based upon a minimum energy error is used in the RKPM formulation. In order to highlight the directional dependence of the phase error, the phase speed is presented with both polar and Cartesian plots. The phase speed results exhibit angular symmetry about propagation directions, θ, that are multiples of $\pi/4$ as a result of the imposed uniform spacing of particles. However, the data is presented for $0 \leq \theta \leq 2\pi$ for the sake of clarity.

3.2.1 First-Order Wave Equation

Phase speed plots for the semi-discrete first-order wave equation using the fully integrated bi-linear finite element and a consistent mass matrix are shown in Figure 6. The polar plot of Figure 6a shows phase speed as a function of direction, θ, for several values of non-dimensional wavelength, $2\Delta x/\lambda$. The non-circular phase speed contours emphasize the anisotropic nature of wave propagation on the discrete mesh. Figure 6b presents the results of Figure 6a at five propagation angles, θ. It is apparent from Figure 6 that a minimum error in phase speed occurs when the wave propagation direction is $\pi/4$ from the x-axis. It is also apparent that the anisotropy becomes more pronounced for shorter wavelengths, i.e., $2\Delta x/\lambda > 0.4$ (cf. Figure 6a).

Phase speed results for the fully integrated "bi-linear" reproducing kernel particle method using a consistent mass matrix are shown in Figure 7. As with the FE formulation, the RKPM semi-discretization leads to strictly lagging phase speed with minimum phase speed errors occurring for $\theta = \pi/4$. However, unlike FE, RKPM shows negligible phase error in this direction. Further, relative to the finite element method, the anisotropic behavior has been significantly reduced, with wave propagation being effectively independent of wavelength and propagation direction for $2\Delta x/\lambda \leq 0.8$, i.e., for wavelengths greater than about $2 - 3\Delta x$.

Figure 8 shows polar and Cartesian plots of the phase speed for the "bi-linear" RKPM formulation using trapezoidal integration and a consistent mass matrix. Again, the phase speed is lagging and anisotropic, with minimum errors occurring in the $\theta = \pi/4$ directions. Although the phase speed appears anisotropic for short wavelength signals, this formulation delivers nearly isotropic wave propagation for $2\Delta x/\lambda \leq 0.6$, i.e., wavelengths greater than $3 - 4\Delta x$.

3.2.2 Second-Order Wave Equation

Figure 9 shows phase speed results for the second-order wave semi-discretization using a fully integrated bi-linear finite element method with a consistent mass matrix. The results indicate that the finite element formulation introduces strictly leading phase errors. The finite element semi-discretization results in anisotropic wave propagation, with a minimum phase error occurring in the $\theta = \pi/4$ propagation directions. However, the anisotropy is not as pronounced as for the first-order equation (cf. Figure 6)

The fully integrated "bi-linear" RKPM semi-discretization (consistent mass matrix) yields almost negligible phase errors as shown in Figure 10. Further, as phase errors are quite small for all θ, wave propagation is nearly perfectly isotropic. Some slight leading phase speed errors are evident for wavelengths approaching $2\Delta x$. However, these errors are less than 2.5% with a minimum in phase error occurring in the $\theta = \pi/4$ propagation directions.

Finally, Figure 11 shows the phase speed results for "bi-linear" RKPM semi-discretization using trapezoidal integration with a consistent mass matrix. Unlike the fully integrated results, anisotropic dispersion errors are quite evident for $2\Delta x/\lambda > 0.6$. However, for $2\Delta x/\lambda \leq 0.6$ phase errors are negligible and are significantly better than for the FE case (cf. Figure 9). Similar to the fully-integrated RKPM semi-discretization, the phase errors are minimized in the $\pi/4$ propagation directions, but with nearly perfect phase speed for wavelengths longer than $3 - 4\Delta x$.

Remark

> During the course of analyzing the results from the von Neumann analysis it was observed that the use of trapezoidal integration results in identical dispersion relations for the first and second-order wave equations with a consistent mass matrix. The fact

that the discrete spectrum or *symbol*[20] for the first and second-order wave equations are identical may be seen clearly in Figures 3 and 5 for the one-dimensional case. Similarly, for the two-dimensional case, the phase speed shown for the first-order wave equation in Figure 8 is identical to the phase speed shown in Figure 11.

Similar behavior has been noted by Vichnevetsky and Bowles[20] when a second-order central difference approximation is applied to both the first and second-order wave equation. In this situation, the semi-discrete first-order equation is a consistent representation of the second-order wave equation. In the case of RKPM, a similar result may be obtained in the one-dimensional case for a refinement parameter, $r = 1/2$. However, we have been unable to to verify this behavior analytically for $r = 1.14$. Regardless of this, numerical experiments (cf. Figures 3, 5, 8, and 11 have verified that the discrete spectrum is identical for the two model hyperbolic equations when particle integration is used.

4 Summary and Conclusions

This paper presents a dispersion analysis for RKPM semi-discretizations of two model hyperbolic partial differential equations. The semi-discretizations considered incorporate linear or bi-linear consistency (one or two-dimensional forms respectively) and use variations on matrix integration (full Gauss quadrature or particle integration) and type (consistent, lumped or higher order). All formulations incorporate a cubic-spline kernel function with the optimal refinement parameter of $r = 1.14$.

The results of the analyses presented here indicate that, for the formulations considered, the consistent mass RKPM-CF semi-discretizations display better dispersion properties than the finite element method with similar consistency constraints. In a one-dimensional sense, phase errors of less than 5% are ensured with 3 to 4 particles per wavelength with RKPM while the FE formulations require 4 to 5 nodes. Incredibly, RKPM semi-discretizations of the second-order wave equation require only 3 particles per wavelength (the Nyquist limit) for phase errors of less than 2.5 percent. In addition, wave propagation with the consistent mass RKPM formulation in two-dimensions is nearly isotropic in terms of angular dependence of the phase speed and in

terms of the amplitude of the phase errors.

While the consistent mass matrix RKPM formulations perform quite well, the lumped and higher order mass formulations introduce severely lagging phase and group speeds. Thus, the performance of these formulations is quite poor relative to their FE counterparts.

Finally, the consistent mass RKPM results indicate that minimal losses in phase and group speed error result when particle integration of the matrices is employed in place of full (Gauss) quadrature. With the sacrifice of negative group speeds and a slight increase in phase speed errors, the use of particle integration may significantly reduce computational cost by reducing the number of quadrature points needed. Further, the method should be simpler to implement as the background integration mesh can be eliminated. However, further direct testing with particle integration is required.

Acknowledgments

The authors would like to thank Professor Wing Kam Liu for his assistance in understanding reproducing kernel particle methods, and Darin Diachin and Shawn Burns for providing helpful suggestions in the development of this manuscript.

References

[1] T. Belytschko, Y. Krongauz, D. Organ, M. Fleming, and P. Krysl, *Meshless methods: An overview and recent developments*, Computer Methods in Applied Mechanics and Engineering, 139 (1996), pp. 3–47.

[2] J.-S. Chen, S. Yoon, H.-P. Wang, and W. K. Liu, *An improved reproducing kernel particle method for nearly incompressible hyperelastic solids*, submitted to Computer Methods in Applied Mechanics and Engineering, (1997).

[3] Y. Chen, R. A. Uras, and W. K. Liu, *Enrichment of the finite element method with reproducing kernel particle method*, in Joint ASME/JSME pressure vessels and piping conference, ASME/JSME, July 1995.

[4] M. A. CHRISTON, *The influence of the mass matrix on the dispersive nature of the semi-discrete, second-order wave equation*, Computer Methods in Applied Mechanics and Engineering, (accepted for publication, June, 1998).

[5] S. JUN, W. K. LIU, AND T. BELYTSCHKO, *Explicit reproducing kernel particle methods for large deformation problems*, International Journal for Numerical Methods in Engineering, (Accepted for publication - March,1997).

[6] S. LI AND W. K. LIU, *Moving least square reproducing kernel method part ii: Fourier analysis*, Computer Methods in Applied Mechanics and Engineering, 139 (1996), pp. 159–193.

[7] ——, *Synchronized reproducing kernel interpolant via multiple wavelet expansion*, Computational Mechanics, (Accepted for publication March, 1997).

[8] ——, *Moving least square reproducing kernel method (iii): Wavelet packet and its applications*, Computer Methods in Applied Mechanics, (submitted April, 1997).

[9] W. K. LIU AND Y. CHEN, *Wavelet and multiple scale reproducing kernel methods*, International Journal for Numerical Methods in Fluids, 21 (1995), pp. 901–931.

[10] W. K. LIU, Y. CHEN, C. T. CHANG, AND T. BELYTSCHKO, *Advances in multiple scale kernel particle methods*, Computational Mechanics, 18 (1996), pp. 73–111.

[11] W. K. LIU, Y. CHEN, J. S. CHEN, T. BELYTSCHKO, C. PAN, R. A. CURAS, AND C. T. CHANG, *Overview and applications of the reproducing kernel particle methods*, Archives of Computational Methods in Engineering, 3 (1996), pp. 3–80.

[12] W. K. LIU, Y. CHEN, R. A. URAS, AND C. T. CHANG, *Generalized multiple scale reproducing kernel particle methods*, Computer Methods in Applied Mechanics and Engineering, 139 (1996), pp. 91–157.

[13] W. K. Liu and S. Jun, *Multiple scale reproducing kernel particle methods for large deformation problems*, International Journal for Numerical Methods in Engineering, (submitted 1997).

[14] W. K. Liu, S. Jun, S. Li, J. Adee, and T. Belytschko, *Reproducing kernel particle methods for structural dynamics*, International Journal for Numerical Methods in Engineering, 38 (1995), pp. 1655–1679.

[15] W. K. Liu, S. Jun, and Y. F. Zhang, *Reproducing kernel particle methods*, International Journal for Numerical Methods in Fluids, 20 (1995), pp. 1081–1106.

[16] W. K. Liu, S. Li, and T. Belytschko, *Moving least square reproducing kernel methods (i) methodology and convergence*, Computer Methods in Applied Mechanics and Engineering, (Accepted for publication - June, 1996).

[17] W. K. Liu and C. Oberste-Brandenburg, *Reproducing kernel and wavelet particle methods*, in Aerospace Structures: Nonlinear dynamics and system response, J. P. Cusumano, C. Peirre, and S. T. Wu, eds., New York, New York, November 1993, ASME Winter Annual Meeting, American Society of Mechanical Engineers, pp. 39–55.

[18] R. A. Uras, C. T. Chang, Y. Chen, and W. K. Liu, *Multiresolution reproducing kernel particle methods in acoustics*, Journal of Computational Acoustics, (Accepted for publication, 1996).

[19] R. Vichnevetsky, *Wave propagation and reflection in irregular grid for hyperbolic equations*, Tech. Rep. MAE-1713, Department of Mechanical and Aerospace Engineering, Princeton University, July 1985.

[20] R. Vichnevetsky and J. B. Bowles, *Fourier Analysis of Numerical Approximations of Hyperbolic Equations*, SIAM, Philadelphia, PA, 1982.

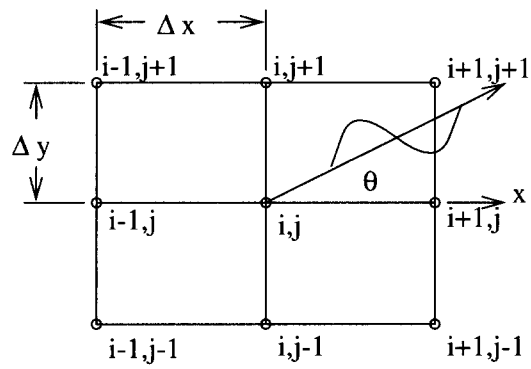

Figure 1: Particle distribution and wave propagation direction, θ, for the dispersion analysis.

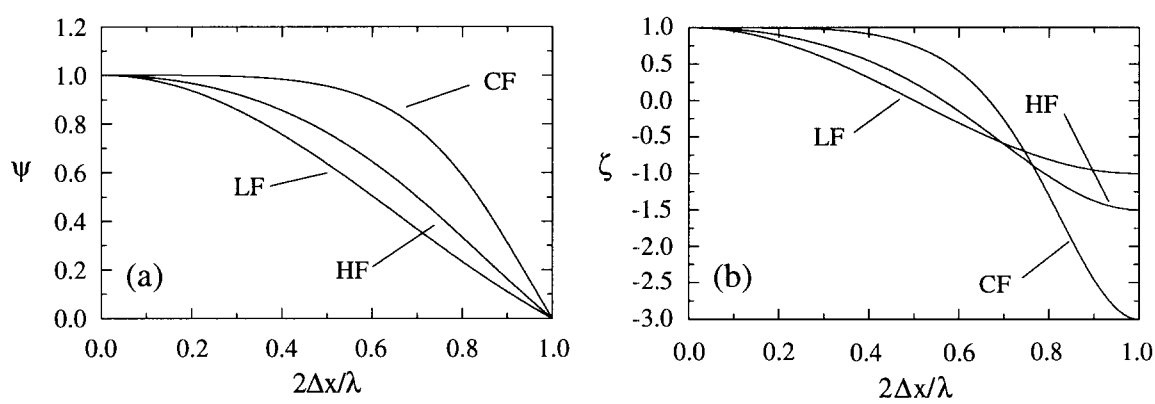

Figure 2: One-dimensional phase (a) and group (b) speed results for the first-order wave, linear finite element semi-discretization employing fully integrated, consistent (CF), lumped (LF) mass and higher-order (HF) matrix formulations.

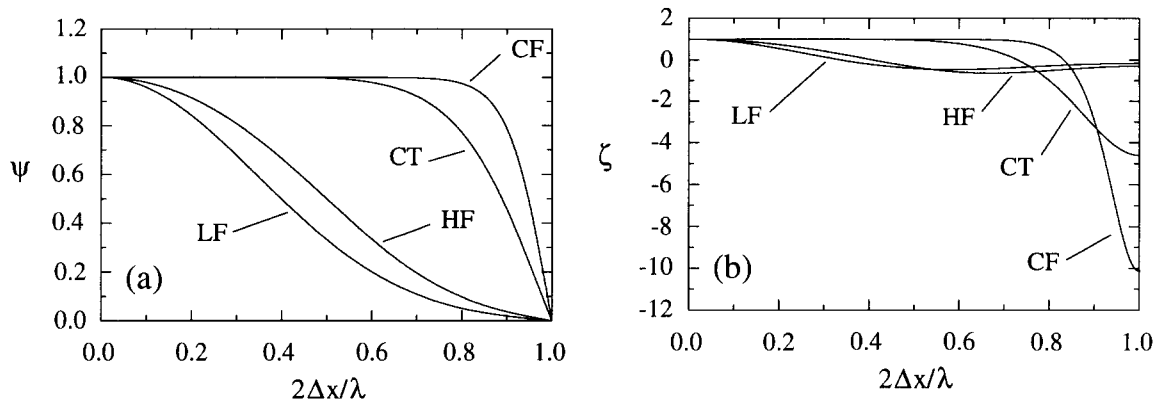

Figure 3: One-dimensional phase (a) and group (b) speed results for the first-order wave, Reproducing Kernel Particle semi-discretization employing full-integration consistent (CF), lumped (LF), higher-order (HF) and trapezoidal integration consistent (CT) mass matrix formulations.

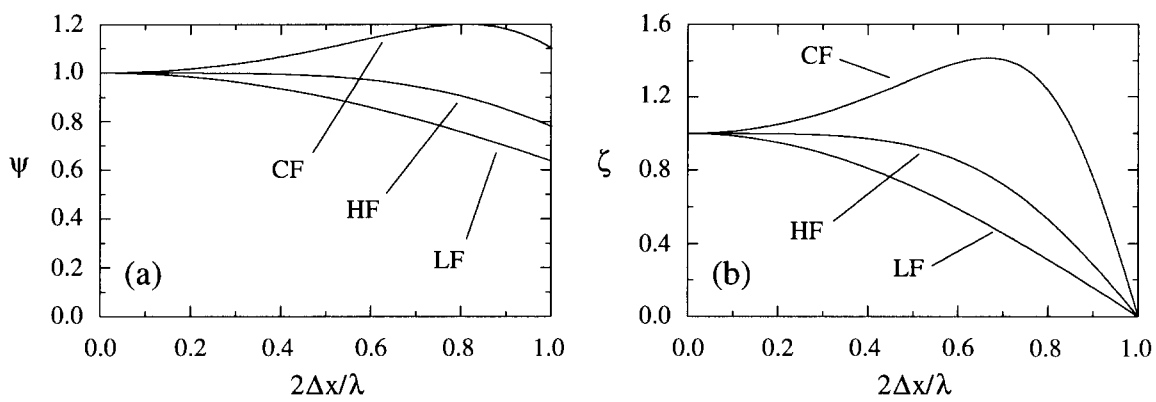

Figure 4: One-dimensional phase (a) and group (b) speed results for the second-order wave, linear finite element semi-discretization employing full-integration consistent (CF), lumped (LF) and higher-order (HF) mass matrix formulations.

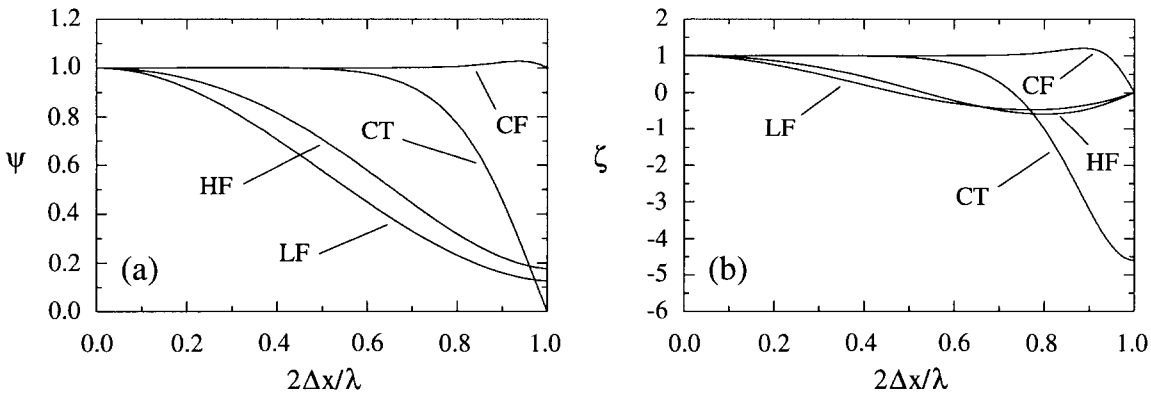

Figure 5: One-dimensional phase (a) and group (b) speed results for the second-order wave, Reproducing Kernel Particle semi-discretization employing the full-integration, consistent (CF), lumped (LF), higher-order (HF) and trapezoidal integration consistent (CT) mass matrix formulations.

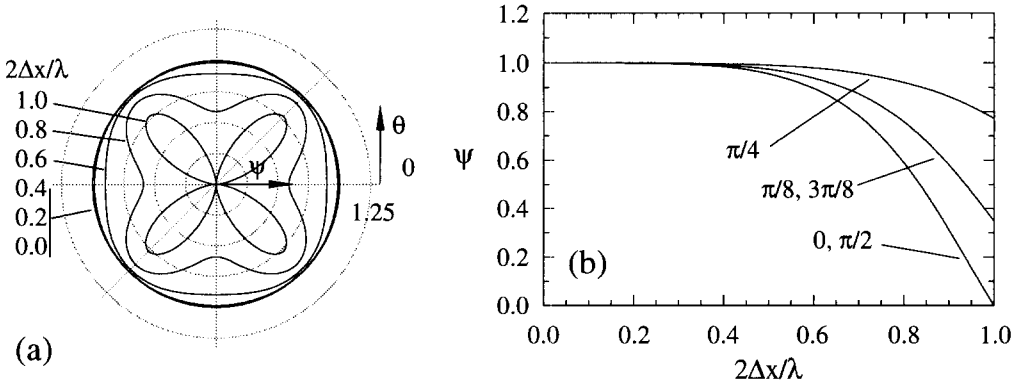

Figure 6: Polar (a) and Cartesian (b) plots of the phase speed for the FE semi-discretization of the two-dimensional, first-order wave equation employing a full-integration, consistent mass matrix formulation (CF).

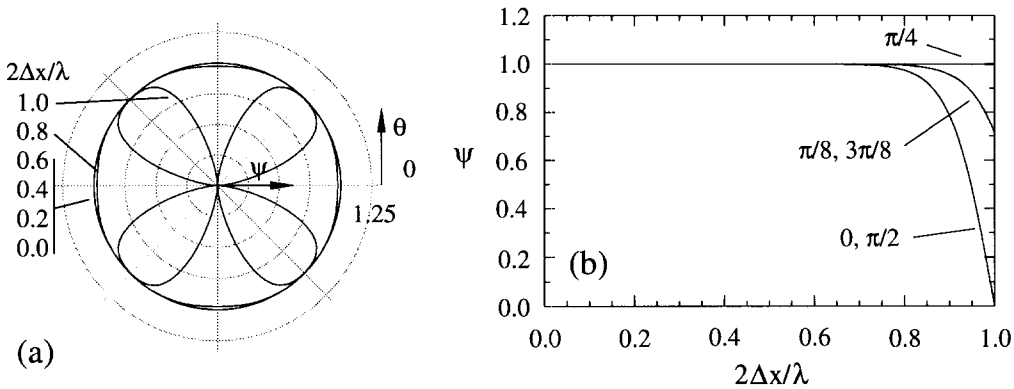

Figure 7: Polar (a) and Cartesian (b) plots of the phase speed for the RKPM semi-discretization of the two-dimensional, first-order wave equation with full-integration, and a consistent mass matrix (CF).

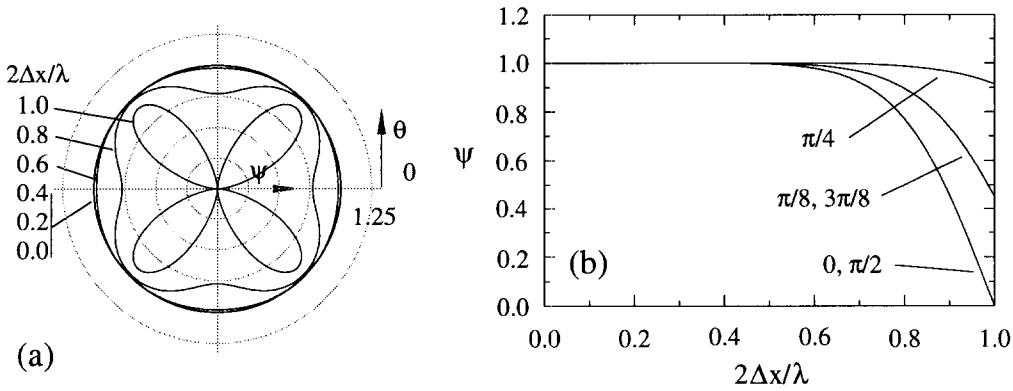

Figure 8: Polar (a) and Cartesian (b) plots of the phase speed for the RKPM semi-discretization of the two-dimensional, first-order wave equation with a consistent mass matrix and trapezoidal integration (CT).

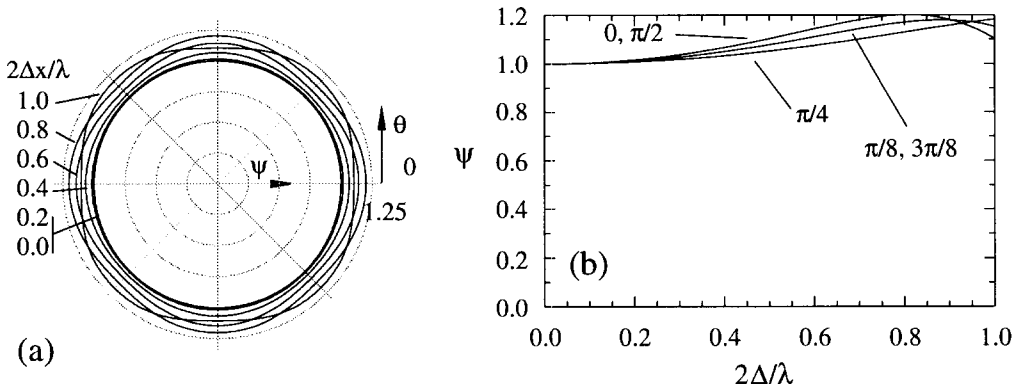

Figure 9: Polar (a) and Cartesian (b) plots of the phase speed for the FE semi-discretization of the two-dimensional, second-order wave equation using a full-integration, consistent mass matrix formulation (CF).

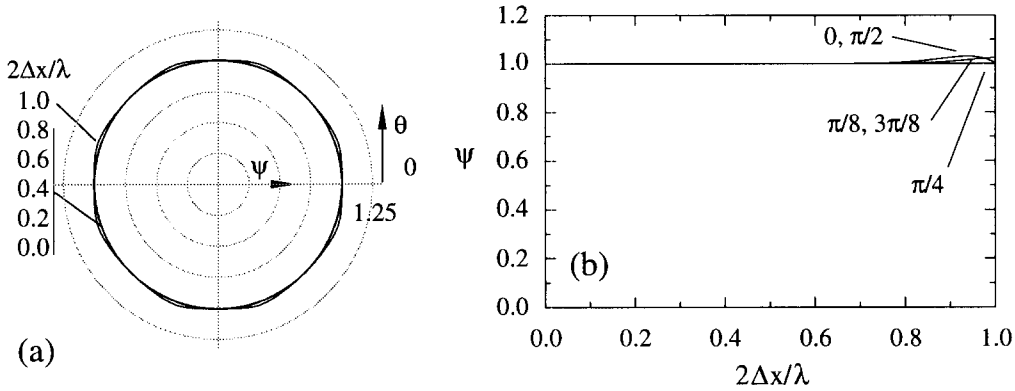

Figure 10: Polar (a) and Cartesian (b) plots of the phase speed for the RKPM semi-discretization of the two-dimensional, second-order wave equation using full-integration and a consistent mass matrix (CF).

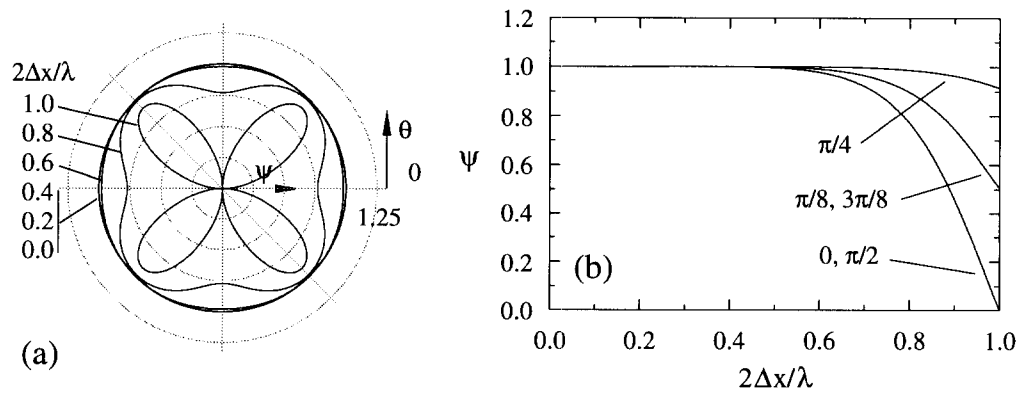

Figure 11: Polar (a) and Cartesian (b) plots of the phase speed for the RKPM semi-discretization of the two-dimensional, second-order wave equation using a consistent mass matrix and trapezoidal integration (CT).